ANALYSIS OF COPLANAR WAVEGUIDE BY THE TIME-DOMAIN FINITE-DIFFERENCE METHOD

G. C. Liang, Y. W. Liu, and K. K. Mei

Department of Electrical Engineering and Computer Sciences and the Electronics Research Laboratory
University of California, Berkeley, CA 94720

ABSTRACT

An analysis of coplanar waveguides (CPW) by the Time-Domain Finite Difference (TD-FD) method is discussed. The propagating waveforms along a coplanar waveguide, which is excited by a Gaussian pulse, are found in the time-domain. After the time-domain computation is done, the frequency domain parameters, such as the effective dielectric constant and the complex characteristic impedance, are calculated by Fourier transformations. The results agree well with the available theoretical and experimental data over a wide frequency range.

Introduction

The CPW has been studied by several investigators and all the work is done in the frequency domain. Analyses on CPW have been carried out using Galerkin's method in the spectrum-domain [1-2], in which a simplified Fourier transformable current distribution is assumed. The time-domain method to be discussed in this paper is a complete full-wave analysis, with no computational assumptions other than the equation discretization and mesh termination. The method is quite general and is applicable, for example, to microstrip lines [3], coplanar strips, slot lines [4], and coplanar waveguides. The method is also being used to analyze superconductive transmission lines, where the superconductive electrode dispersions, the geometrical dispersions, the modal dispersions, and the radiation effects are all taken into consideration.

The time-domain method is easy to apply. Using this method, we first find the propagating waves along the coplanar waveguide in the time domain; Fourier transforms are then applied to the time-domain results to obtain frequency domain design parameters, such as the characteristic impedances, the propagation velocities, and the effective dielectric constants. The main issues are presented and discussed in the subsequent sections.

Pulse Excitation

A retarded Gaussian pulse is used as an excitation. The spatial distribution of the excitation pulse on the excitation plane is also considered. We use a quasi-static approximated field pattern as the initial distribution in the present study. It is observed that the different choices of the spatial distribution affect only the amount of time taken to reach the stable solution, not the solution itself. The complete excitation pulse at $t = t_n$ can be written as:

$$E_x(x,y,t_n) = \Psi_x(x,y) \exp\left[-\frac{(t_n - t_0)^2}{T^2}\right] \quad (1)$$

and

$$E_y(x,y,t_n) = \Psi_y(x,y) \exp\left[-\frac{(t_n - t_0)^2}{T^2}\right] \quad (2)$$

where $\Psi_x(x,y)$ and $\Psi_y(x,y)$ are the previously mentioned pulse spatial distributions, t_0 is the initial time delay, and the pulsewidth parameter T is mainly subjected to the frequency range concerned.

Boundary Truncation

Boundary truncation must be done to carry out numerical simulation on an open-structured CPW. Field distributions along the CPW are not as localized as those of microstrips, thus making the boundary conditions more difficult to handle. The front plane of the computation domain is the plane of the excitation and the fields $E_x(x,y,t)$, and $E_y(x,y,t)$ on it are specified by Eqs. (1) and (2). The plane of symmetry is replaced by an electric wall so that only half of the region needs to be considered. The other four planes have to be substituted by the proper "absorbing boundary walls" to make the computation feasible. The boundary treatment in the present research is mainly based on reflection error cancellations [5].

Field Components Calculation

Yee's TD-FD method [6] is employed to solve Maxwell's equations. Different field components occupy the different nodal points on the lattices. Starting from the initial field, the electric and magnetic fields within the computation domain, which is filled with Yee's lattice, can be evaluated at alternate half-time steps from the discretized forms of Maxwell's equations.

Frequency Parameter Evaluation

After the time-domain calculations are done, we can find the related frequency parameters using the single-mode model. The propagation constant for section $\overline{z_i z_j}$ on the

CPW can be expressed as:

$$\gamma(\omega,\overline{z_i z_j}) = \frac{1}{z_j - z_i}\ln\left\{\frac{W(\omega,z_i)}{W(\omega,z_j)}\right\} \tag{3}$$

where $W(\omega,z_i)$ and $W(\omega,z_j)$ are the Fourier transforms of the E or H field components sampled at $z = z_i$ and $z = z_j$, respectively. The characteristic impedance can be defined as the ratio of the Fourier transforms of the voltage and current:

$$Z(\omega,z_i) = \frac{V(\omega,z_i)}{I(\omega,z_i)} \tag{4}$$

where the voltage and current in Eq. (4) are defined as follows:

$$V(t,z_i) \triangleq \int_a^b \vec{E}(x,y,t,z_i)\cdot d\vec{\xi} \tag{5}$$

$$I(t,z_i) \triangleq \oint_c \vec{H}(x,y,t,z_i)\cdot d\vec{l} \tag{6}$$

where point "a" is located on the edge of the center electrode, and point "b" is on the edge of the side electrode. The loop c encloses the center electrode. The above two integrations have been implemented with different paths or loops. The loop c is a rectangle which encloses the center electrode. Deviations for different pathes are negligible as long as H_z and E_z are not significant, which will be discussed elsewhere.

It is appropriate to distinguish $\gamma(\omega)$ and $Z(\omega)$ obtained from the different segments $\overline{z_i z_j}$ or different points z_i's, since γ 's and Z's evaluated at different locations may not be identical due to the imperfect boundary treatment. The errors caused by imperfect treatment could be reduced by averaging γ 's and Z's obtained at different locations or by using the least squares method.

In the calculations above, the transmission line is terminated by a matched impedance. Actually, we can obtain more precise results for $\gamma(\omega)$ and $Z(\omega)$ by combinations of electric wall (short end) and magnetic wall (open end) terminations, with other boundaries being matched. From the general transmission line equations, it is straightforward to obtain the expressions for $\gamma(\omega)$ and $z(\omega)$ evaluated at $z = \xi_0$ as follows:

$$\gamma(\omega,\xi_0) = \frac{1}{2\xi_0}\ln\left[\frac{[\frac{V(\omega,\xi_0)}{I(\omega,\xi_0)}]_o^{\frac{1}{2}} + [\frac{V(\omega,\xi_0)}{I(\omega,\xi_0)}]_s^{\frac{1}{2}}}{[\frac{V(\omega,\xi_0)}{I(\omega,\xi_0)}]_o^{\frac{1}{2}} - [\frac{V(\omega,\xi_0)}{I(\omega,\xi_0)}]_s^{\frac{1}{2}}}\right] \tag{7}$$

$$Z(\omega,\xi_0) = \left[[\frac{V(\omega,\xi_0)}{I(\omega,\xi_0)}]_o [\frac{V(\omega,\xi_0)}{I(\omega,\xi_0)}]_s\right]^{\frac{1}{2}} \tag{8}$$

where the ratios $[V(\omega,\xi_0)/I(\omega,\xi_0)]_o$ and $[V(\omega,\xi_0)/I(\omega,\xi_0)]_s$ are the ratios of the Fourier transforms of the voltage and current evaluated at $z = \xi_0$ by open and short terminations, respectively. Similar techniques, as previously mentioned, can also be used to reduce the errors of the field components in this algorithm.

Numerical Implementation

Set Up of the Calculation

Coplanar waveguides with different dimensions have been investigated. Their geometric and computation parameters are shown in Table I

Table I

Parameters for CPW	Case a	Case b
Center electrode width W (mm)	0.135	0.4
Electrode space S (mm)	0.065	0.5
Side electrode width W' (mm)	0.59	infinite
Substrate thickness H (mm)	0.5	1.0
Metal strip thickness T (mm)	0.0	0.0
Space step dh (mm)	0.0135	0.050
Time step dt (ps)	0.0176	0.0858
Dielectric constant ε_r	12.9	20.0

In the calculation, the side electrode W' is assumed to be infinite for simplicity. The computation spatial step dh is chosen to accommodate the structure conveniently; the time step dt is chosen to satisfy the stability conditions. The computation domain is a box with sides $(n_1\Delta x)\times(n_2\Delta y)\times(n_3\Delta z)$, which is usually determined by the available memory.

Spatial Fields Distribution

Fig. 1 shows a typical spatial distribution of the fields $E_x(x,y,z,t_n)$ at time step t_n (case a.). The edge effect is shown in the pattern. It is worthwhile to mention that no special treatment is needed on the edge, if only the tangential component $\vec{E}_t$ and normal components $\vec{H}_n$ are posed on the metalized plane.

Time Waveforms of the field components

Instead of taking snapshots of the waves, we can record the field at a fixed point P (ξ_0 , ζ_0 , η_0) in the computation domain. Fig. 2 shows the time waveforms sampled at different z's ($z = i\,\Delta h$, i= 20, 30, 40, 50, 60, 70.). As indicated in Fig. 2, the amplitude of the pulse decreases and its width increases as the pulse propagates along the line, because of radiation and dispersion. The radiation effect is also verified by the fact that the impedance is complex. furthermore, the radiation effect contributes to distortion of the pulse, since components of different frequencies are not equally radiated. The radiation effect on dispersion and attenuation is not accounted for in the spectrum-domain analysis [1-2]. It is also observed that the dc component decays as the pulse propagates along the line.

Surface Current Distributions

The surface current distribution is obtained directly from the tangential magnetic field. Compared with the spectral domain analysis, we do not need to assume the surface current distribution on the metal strips. By taking the Fourier transform of the current obtained in the present calculation, the validity of assumed current distributions, used in the spectral domain analysis within the concerned frequency range, can be checked. It is noteworthy that for the center electrode, the current density distribution reaches its

maximum at the edges and minimum at the center. For the side electrode, the current density has maximum at the inner edges and decays monotonically towards the outer edges. This rate of decay is helpful in determining the size of the enclosure for the CPW. It is observed that the longitudinal current density at the outer edge of the side electrode is practically zero, when $W'/W > 8$ for a CPW with substrate thickness H = 0.52 mm.

Once the surface electric and magnetic currents are found, it is straightforward to find far fields by the following general expressions:

$$\vec{E}(r) = \frac{-j}{\omega\mu\varepsilon} \nabla (\nabla \cdot \vec{A}) - j\omega\vec{A} - \frac{1}{\varepsilon}\nabla\times\vec{F} \tag{9}$$

$$\vec{H}(r) = \frac{1}{\mu}\nabla\times\vec{A} - \frac{j}{\omega\mu\varepsilon}\nabla(\nabla\cdot\vec{F}) - j\omega\vec{F} \tag{10}$$

with

$$\vec{A} = \frac{\mu}{4\pi}\iint_s \vec{K}(r') \frac{e^{-jk_0|\vec{r}-\vec{r}'|}}{|\vec{r}-\vec{r}'|} ds' \tag{11}$$

$$\vec{F} = \frac{\varepsilon}{4\pi}\iint_s \vec{M}(r') \frac{e^{-jk_0|\vec{r}-\vec{r}'|}}{|\vec{r}-\vec{r}'|} ds' \tag{12}$$

where $\vec{K}(r')$ and $\vec{M}(r')$ are surface electric and magnetic currents, respectively. It is clear that the time-domain method can be readily modified to deal with patch antenna problems.

Dispersion Relations

As discussed above, dispersion relations can be found according to eq. (3). Figure 3(a) shows the comparisons of effective dielectric constant $\varepsilon_{effect}(f)$ for case a. Curve 1 is the result of present calculations. Curve 2 is from the empirical formula obtained by the spectrum-domain analysis [2]. They agree well with each other up to 120 GHz. The five dots are experimental data by pulse (harmonic-mixing) electro-optic probing techniques [7]. It is also in good agreement with those numerical results ranging from 4.11 GHz to 20.1 GHz. Figure 3(b) shows the similar plot for case b. Curve 1 is the present result. Curve 2 is from ref. [2]. Curve 3 is the theoretical result from ref. [8]. As can be seen, the first two results are in good agreement up to 17 GHz for the given geometry. The effective dielectric constant in [8] is slightly smaller than the other two.

Frequency-Dependent Characteristic Impedances

The frequency dependent characteristic impedance is found by Eq. (4). The dc value is close to that obtained by the quasi-static analysis for both cases a and b. The real part of impedance is quite flat up to 150 GHz for case a. The imaginary part is due to radiation. Figure 4(a) and (b) show the complex impedance for case a and b respectively. In these plots z_r and z_i are the real and imaginary parts of the complex impedance respectively. In Fig. 4(b), z_0 is the real impedance from [8].

Summary and Conclusion

The coplanar waveguide has been analyzed by the TD-FD method. The time and frequency results have been presented and explained. Frequency parameters are in good agreement with those from the spectrum-domain analysis method by Kitazawa [8] and the experimental data.

Acknowledgement

This work was supported in part by Joint Services Electronics Program under contract number: F49620-87-C-0041, and by Microelectronics Innovation and Computer Research Opportunities under proposal number: 88-111. The authors wish to thank J. Y. Fang and X. L. Zhang for helpful discussion.

References

[1] J. B. Knorr, K. D. Kuchler, "Analysis of Coupled Slots and Coplanar Strips on Dielectric Substrate," *IEEE Trans. Microwave theory Tech.*, Vol. MTT-23, pp. 541 - 548 , July, 1975.

[2] G. Hasnain, A. Dinenes, and J. R. Whinnery, "Dispersion of picosecond pulses in coplanar transmission lines," *IEEE Trans. Microwave Theory Tech.*, Vol. MTT-34, No.6, pp. 378-741, June. 1986.

[3] X. Zhang, J. Fang, K. K. Mei and Y. Liu "Calculation of the Dispersion Characteristics of Microstrips by the Time-Domain Finite Difference Method," *IEEE Trans. Microwave Theory Tech.*, Vol. MTT-36, No. 2, pp. 263-267, Feb. 1988.

[4] G. C. Liang, Y. W. Liu, K. K. Mei "On the Characteristics of the Slot Lines," to be published in 1989 IEEE AP-S International Symposium. San Jose, California, June 26-30, 1989

[5] K. K. Mei and J. Fang "Super-absorption: a method to improve local absorbing boundary condition," Submitted for Publication in *J. Compu Physics*

[6] K. S. Yee, "Numerical solution of initial boundary value problems involving Maxwell's equations in isotropic media," *IEEE Trans. Antenna Propagat.*, AP-14, pp. 302-307, May 1966.

[7] Z. H. Zhu, M. C. Wu, Y. H. Lo, C. L. Pan, S. Y. Wang, and S.Wang, "Measurements on standing waves in GaAs coplanar waveguide at frequencies up to 20.1 GHz by electro-optic probing," *J. Appl. Phys.*, Vol 64 No. 1, pp. 419-421, July 1988.

[8] T. Kitazawa, Y. Hayashi, and M. Suzuki, "A coplanar Waveguide with the metal-coating," *IEEE Trans. Microwave Theory Tech.*, Vol. MTT-24, No. 2, pp. 604-608, Sept. 1976.

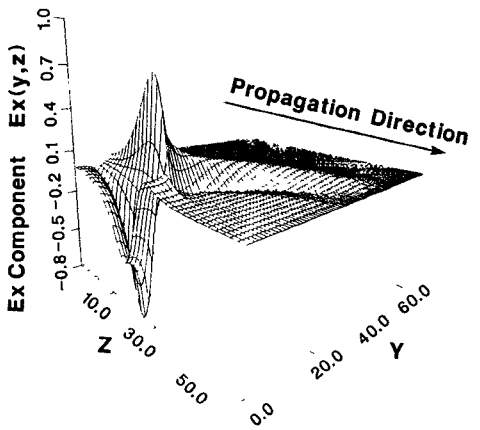

Fig. 1 The spatial waveforms of E_y, which is sampled just below the electrodes.

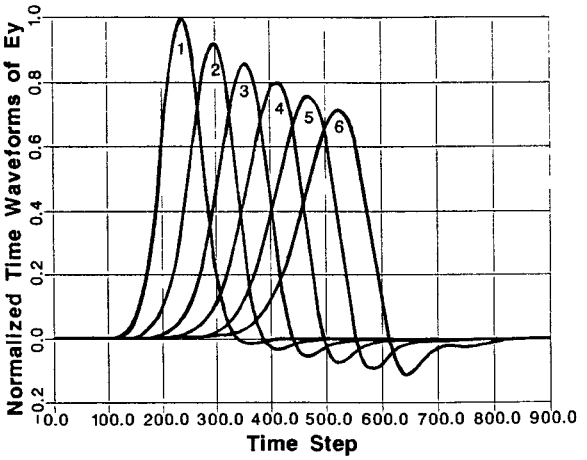

Fig. 2 Normalized time waveforms of E_y at different z's. These signals are sampled below the center electrode.

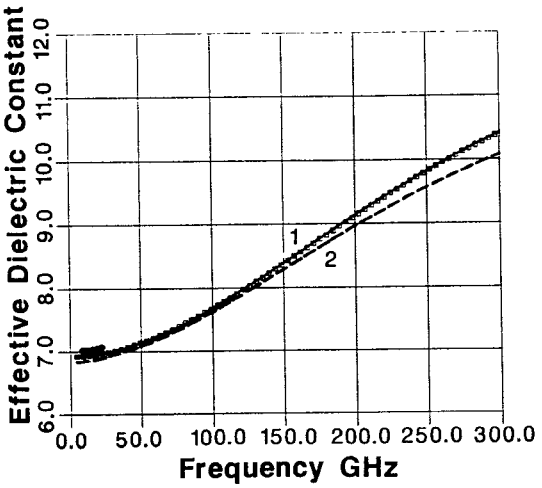

Fig. 3 (b) Comparison of the calculated result of effective dielectric constant for case b. Curve 1 is the present result. Curve 2 is from [2]. Curve 3 is the theoretical data form the ref.[8].

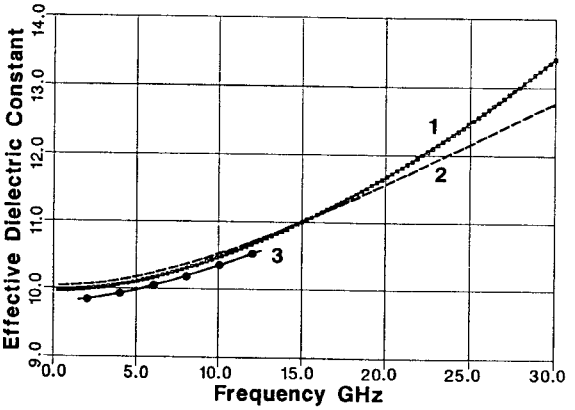

Fig. 3 (a) Comparison of the effective dielectric constant for case a. Curve 1 is the present result. Curve 2 is from [2]. The five points are experimental data [7].

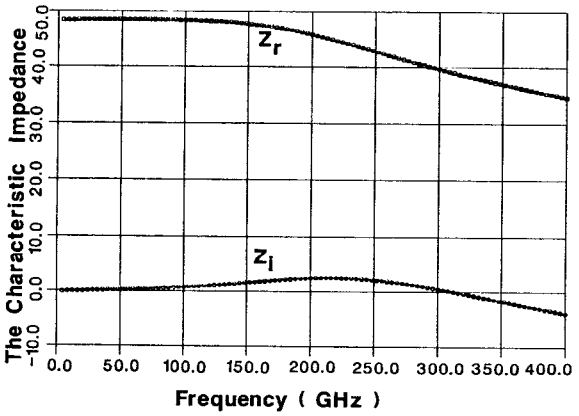

Fig. 4 (a) Complex characteristic impedance for case a. Z_r and Z_i are the real and imaginary parts of the impedance.

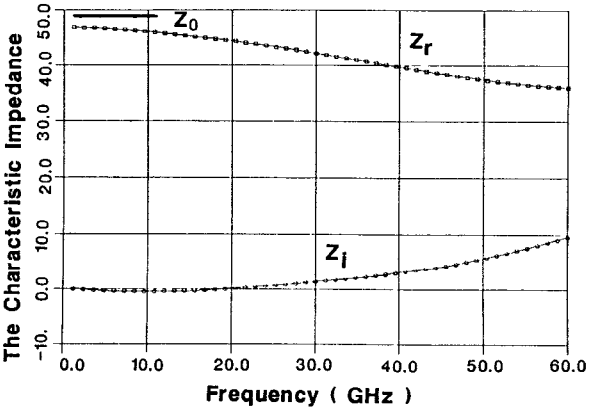

Fig. 4 (b) Complex characteristic impedance for case b. Z_r and Z_i are the real and imaginary parts of the impedance. Z_0 is the real characteristic impedance from ref. [8]